Journal of Power Sources 614 (2024) 234978

Contents lists available at ScienceDirect

Journal of Power Sources

journal homepage: www.elsevier.com/locate/jpowsour

Effect of cathode ink formulation on the hydrogen crossover and cell performance of proton exchange membrane water electrolyzers

Inku Kang [a], Won-Jong Choi [a], Hwan Yeop Jeong [a], Chang Jin Lee [a], Soonyong So [a], Duk Man Yu [a], Sang Jun Yoon [a], Hongsuk Kang [b], Dong-Won Kim [c,d,**], Keun-Hwan Oh [a,*]

[a] Hydrogen Energy Research Center, Korea Research Institute of Chemical Technology, 141 Gajeong-ro, Yuseong-gu, Daejeon, 34114, Republic of Korea
[b] Program in Environmental and Polymer Engineering, Department of Polymer Science and Engineering, Inha University, Incheon, 22212, Republic of Korea
[c] Department of Chemical Engineering, Hanyang University, Seoul, 04763, Republic of Korea
[d] Department of Battery Engineering, Hanyang University, Seoul, 04763, Republic of Korea

HIGHLIGHTS

- Cathode catalyst layers prepared by incorporating polytetrafluoroethylene (PTFE)
- Four distinct types of ionomers integrated into the cathode catalyst layers
- The H_2 fraction in the anode correlated with the cathode catalyst layer structure
- The effects of both PTFE content and ionomer type on H_2 crossover examined

ARTICLE INFO

Keywords:
Hydrogen supersaturation concentration
Polytetrafluoroethylene
Ionomer
Cathode catalyst layer
Hydrogen permeation rate
Proton exchange membrane water electrolyzer

ABSTRACT

The permeation of H_2 through the membranes of proton exchange membrane water electrolyzers (PEMWEs) is a critical safety concern because of the risk of explosion when H_2 mixes with O_2 at the anode and increases in concentration. In this study, we investigated the modification of the cathode catalyst layer in the membrane electrode assembly as a strategy for achieving the safe operation of PEMWEs. The effects of the polytetrafluoroethylene (PTFE) content and type of ionomer in the cathode catalyst layer on the dissolved H_2 concentration, H_2 crossover, and electrochemical performance were investigated. The lowest dissolved H_2 concentration and H_2 permeation rate were achieved when 8 wt% PTFE was used. Consequently, the H_2 volume fraction in O_2 at the anode was less than 0.88 %. Additionally, using the Nafion ionomer (D520, ion exchange capacity: 1 mmol g^{-1}), H_2 volume fractions of 1.27 % and 1.34 % were obtained at 0.08 and 5 A cm^{-2}, respectively. These values are below the lower explosion limit of H_2 in O_2 (4 %), implying that the PEMWE can be safely operated in the low-to-high current density range under ambient pressure. These results provide key guidelines for the design of high-safety cathode catalyst layers for PEMWEs.

1. Introduction

The membrane-electrode assembly (MEA), which is an essential part of proton exchange membrane water electrolyzers (PEMWEs), consists of a proton exchange membrane (PEM), catalyst layer (CL), and porous transport layer (PTL). The PEM facilitates ion transfer between electrodes, whereas the CL, which contains a catalyst and ionomer, facilitates electrochemical reactions. Meanwhile, the PTL ensures a steady water supply and the efficient discharge of generated gases [1–3].

The permeation of H_2 through the PEM toward the anode not only reduces the efficiency of PEMWEs but also presents a critical safety concern. This is because of the significant risk of explosion when H_2 mixes with O_2 at the anode and increases in concentration, with the lower explosion limit (LEL) being 4 mol%–mol% H_2 in O_2 [4,5]. This increase in H_2 concentration in the presence of O_2 is particularly notable at low current densities and becomes more prominent in hydrophilic channels [6–11].

Strategies to reduce the H_2 content in O_2 in PEMWEs have been

* Corresponding author.
** Corresponding author. Department of Chemical Engineering, Hanyang University, Seoul 04763, Republic of Korea.
E-mail addresses: dongwonkim@hanyang.ac.kr (D.-W. Kim), khoh@krict.re.kr (K.-H. Oh).

https://doi.org/10.1016/j.jpowsour.2024.234978
Received 1 April 2024; Received in revised form 2 June 2024; Accepted 25 June 2024
Available online 1 July 2024

extensively investigated [12–17]. Garbe et al. studied the influence of operating parameters such as pressure, temperature, current density, and membrane thickness, on PEMWE efficiency. They systematically examined the causes of voltage reduction and established safe operating current ranges under various conditions via H_2 permeability measurements [18]. Lee et al. demonstrated that H_2 permeability can be reduced by biaxially stretching the PEM, thereby increasing the tortuosity of the hydrophilic channels [7]. Choi et al. synthesized a poly(*para*-phenylene) multiblock polymer using oligomeric chain extenders, which enhanced the chemical and mechanical properties of the polymer while limiting H_2 crossover and expanding the operational current range [19]. Albert et al. developed a styrene- and acrylonitrile-grafted PEM and compared its mechanical properties, areal resistance, H_2 permeability, and safety with those of fluorinated membranes with varying thicknesses. They also engineered a membrane with a lower gas permeability than those of the fluorinated membranes Nafion 115 and Nafion 117 by incorporating a crosslinking agent [20]. Qelibari et al. reinforced a porous poly(ether ether ketone) membrane by injecting it with a sulfonated polyphenylene oxide electrolyte. This membrane exhibited lower H_2 permeability and ohmic resistance than Nafion 115, while demonstrating high durability [21]. Abbas et al. introduced a Pt-recombination interlayer into a PEMWE at a loading range of 1–140 $\mu g_{Pt}\ cm^{-2}$ to impede the permeation of H_2 toward the anode CL. This extended the operational range of the PEMWE, and an optimal loading of 10 $\mu g_{Pt}\ cm^{-2}$ proved to be cost effective and prevented the explosion of gas mixtures at the anode [22]. Similarly, Ito et al. employed a Pt-containing anode CL to facilitate H_2/O_2 recombination, which consumed more than 70 % of the permeated H_2 flux at the anode CL [23]. As exemplified by the above-mentioned studies, reducing H_2 permeability often involves adjusting the membrane thickness or composition, optimizing filler materials, and using precise coating methods. However, these approaches may compromise cell performance owing to the presence of high concentrations of foreign materials. Consequently, cost-effectiveness and cell efficiency are reduced owing to increased expenses and thicker membranes [16], ultimately decreasing the H_2 production efficiency.

To develop a novel approach for reducing H_2 permeability, we focused on the properties of the cathode CL. Once H_2 gas is produced, it traverses the ionomer within the CL and is stored in an external tank. During this transition, H_2 remains within the ionomer for an extended duration, and if the quantity of generated and accumulated H_2 exceeds that of the released H_2, the ionomer becomes saturated with H_2. This condition is known as H_2 supersaturation, and as its magnitude increases, the permeation of H_2 through the PEM also increases. This is because the supersaturation of the dissolved gas in the ionomer film imposes constraints on mass transfer, resulting in increased gas permeation [15,24,25].

Based on this background, the present study aimed to modulate the H_2 content in O_2 gas at the anode by adjusting the ion exchange capacity (IEC) of the ionomer and varying the amount of the hydrophobic additive, polytetrafluoroethylene (PTFE), in the cathode CL. We assessed the impact of the cathode CL structure on the safety of PEMWEs (Fig. 1). Using this approach, the H_2 content in O_2 at 1.5 V was reduced to 0.88 % using 8 wt% PTFE and 1.23 % using the Nafion dispersion (D520) as an ionomer CL. This research offers an effective strategy to enhance PEMWE safety without the need for thicker membranes via the manipulation of the cathode CL properties.

2. Experimental

2.1. Materials

PTFE (60 wt% dispersion in H_2O) and 1-propanol were purchased from Merck (Germany), Nafion membrane (NR212) and Nafion dispersions (D2021, D521, and D520) from Chemours (USA), 3M725 and 3M800 powders from 3M (USA), IrO_2 black from Boyaz Energy (Korea), Pt/C (47.0 wt% Pt, 10V50E) from Tanaka Kikinzoku Kogyo K.K. (Japan), carbon-based gas diffusion layer (GDL; JNT30-A3) from JNTG (Korea), and titanium-based PTL from LT Metal Ltd. (Korea). Deionized water (18 MΩ grade) was obtained using a Milli-DI water purification system (Germany).

2.2. CL fabrication and characterizations

To prepare the anode catalyst ink, a mixture of 0.4 g of IrO_2 black, 0.22 g of Nafion dispersion (D2021), and 0.27 g of 1-propanol and 0.24 g of deionized water as co-solvents was stirred mechanically at 500 rpm

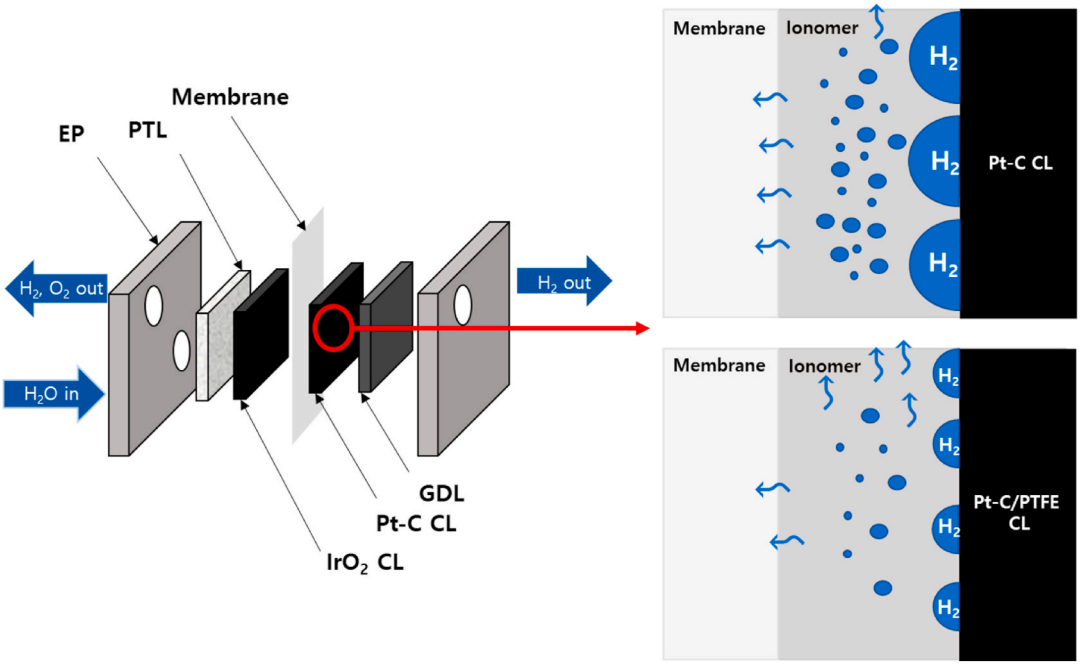

Fig. 1. Schematic representation of supersaturated H_2 within the ionomer of the cathode catalyst layer (CL) and its transport behavior (EP: endplate; PTL: porous transport layer; GDL: gas diffusion layer).

for 2 h. Subsequently, ultrasonic waves were applied for 150 s using a sonicator with a tip. To prepare the cathode catalyst ink, 0.18 g of Pt/C, 1.85 g of ionomer (D521, D520, 3M725, or 3M800), and PTFE were blended using a mechanical stirrer at 500 rpm for 2 h. The PTFE contents were varied as 0, 4, 8, 12, 16, 20, and 24 wt%. The ionomer-to-carbon mass ratio of the cathode catalyst ink was maintained at 1. Subsequently, ultrasonic waves were applied for 210 s using a sonicator with a tip. The evenly dispersed anode or cathode catalyst ink was coated onto a PTFE-coated polyimide film using a 90 μm-gap blade, followed by predrying at 35 °C for 30 min and thorough drying at 80 °C for 2 h.

The morphologies of the cathode CLs were analyzed via field-emission scanning electron microscopy (FE-SEM; GeminiSEM 560, Carl Zeiss) coupled with energy-dispersive X-ray spectroscopy (EDS). The pore size distributions were determined using a mercury intrusion porosimeter (AutoPore V, Micromeritics).

2.3. Measurement of H_2 permeability

Membranes coated with a cathode CL were prepared by thermally bonding a cathode CL to an NR212 membrane using a hot-press machine (CNL, Korea). The permeability (P) of H_2 through the membrane was measured using a test station (SFC-TS, Fuel Cell Technologies Inc.) connected to a gas chromatograph (YL6500 GC, Young In) equipped with a 3 ft column (MolSieve 13X, Agilent) and a thermal conductivity detector (Figs. S1(b) and S1(c)). A membrane was placed between a pair of 210 μm-thick ethylene propylene diene monomer gaskets and flow field plates without gas diffusion layers. Humidified (100 % relative humidity) H_2 and Ar gases at 80 °C were supplied to the anode and cathode sides of the cell, respectively. The carrier gas (Ar) with the permeated H_2 was injected to the gas chromatograph to quantify the concentration of permeated H_2 (C_H) in Ar. P was calculated using the following equation [26]:

$$P = (C_H \times v \times t) \ / \ (A \times \Delta p),$$

where v is the Ar flow rate at standard temperature and pressure (2750 mL min^{-1}); A is the active area through which gas passes (7.5 cm^2); and Δp is the H_2 partial pressure difference across the cathode CL coated membrane. The unit of P is mol m $m^{-2}s^{-1}Pa^{-1}$ (1 mol m $m^{-2}s^{-1}Pa^{-1}$ = 2.987 × 10^{15} barrer) [27].

2.4. Fabrication of catalyst coated membranes (CCMs) and electrochemical characterizations

CCMs were fabricated by decal-transferring an anode or cathode CL (25 cm^2) onto an NR212 membrane at 58.8 MPa and 130 °C for 10 min. After the removal of the polyimide substrate, the catalyst loadings in the anode and cathode CLs were 2.0 mg_{IrO2} cm^{-2} and 0.4 mg_{Pt} cm^{-2}, respectively. A single cell consisting of the CCM, GDL, Ti PTL, two graphitic flow fields with three-serpentine paths, and two endplates was assembled. The clamping torque applied during assembly was 50 kgf cm^{-1}.

The single-cell performance was evaluated by scanning the voltage range from 1.35 to 1.90 V while maintaining a deionized water flow rate of 30 mL min^{-1} at 80 °C under ambient pressure using a water electrolyzer test system (CNL, Korea). Fig. S1(a) illustrates the schematic of the water electrolyzer test station. The voltage was increased incrementally by 0.05 V every 30 s. The H_2 volume fraction was measured with H_2 sensor equipped on the water electrolyzer test system. Electrochemical impedance spectroscopy (EIS; HCP-803, BioLogic) was conducted over a frequency range of 10 kHz to 0.1 Hz using an amplitude of 10 % applied voltage. The proton conduction resistance in the cathode CL of CCMs was determined via EIS. The CCMs were prepared using Pt/C-based CLs with varying PTFE contents and ionomer types. H_2 and N_2 gases were supplied to the anode and cathode CLs, respectively, at flow rates of 200 and 500 mL min^{-1}.

2.5. Calculation of H_2 permeation rate and supersaturation concentration of dissolved H_2

The H_2 permeation rate (P_{H2}) was calculated by combining the H_2 volume fraction (Φ_{H2}) equation with Faraday's law as follows [24]:

$$\Phi_{H2} = \frac{P_{H2}}{P_{H2} + N_{evo,O_2}}, \tag{1}$$

$$N_{evo,O_2} = \frac{i}{4F}, \tag{2}$$

$$P_{H_2} = \frac{i}{4F}\frac{\Phi_{H2}}{1-\Phi_{H2}}, \tag{3}$$

where $N_{evo,O2}$, i, and F are the flux of evolved O_2, applied current density, and Faraday's constant, respectively.

By rearranging the balance equation given in the literature [6], the supersaturation concentration of dissolved H_2 in the ionomer ($C_{H_2}^{super}$) was calculated using the following equation:

$$C_{H_2}^{super} = \frac{\frac{i}{2F} + k_L C_{H2}^{sat}}{k_L + \frac{D_{mem,H_2}}{\delta_{mem}}}, \tag{4}$$

where k_L is the mass transfer coefficient, C_{H2}^{Henry} is the theoretical saturation concentration of dissolved H_2, D_{H2}^{eff} is the effective hydrogen diffusion coefficient of the membrane, and δ_m is the membrane thickness.

Eq. (4) can be inserted into Fick's first law of diffusion to calculate the H_2 permeation rate as follows:

$$P_{H_2} = D_{mem,H_2}\frac{C_{H_2}^{super}}{\delta_{mem}}, \tag{5}$$

The values of these parameters are listed in Table S1.

3. Results and discussion

3.1. Physical properties of cathode CLs

The morphological properties of the cathode CLs were analyzed via SEM and EDS (Fig. 2 and S2). Fig. 2 shows the surface SEM images and C, O, and F elemental maps of the cathode CLs with 0, 8, 16, and 24 wt% PTFE. The SEM images reveal agglomerates composed of the ionomer, catalyst, and PTFE, with sizes varying from a few tens to hundreds of nanometers. The agglomerate size visibly increased with increasing PTFE content owing to the interactions between PTFE and the hydrophobic chains of the ionomer, leading to the formation of a denser polymer coating on the catalyst surface [28,29]. Elemental mapping (Fig. 2 inset) and EDS (right panel of Fig. 2) confirmed the presence of C, O, and F in the cathode CLs. The orange hue representing F in the elemental maps gradually darkened as the PTFE content increased. EDS spectral analysis over the same range showed an increase in the detection frequency of F from 3 to 4.5 cps as the PTFE content increased. This indicates greater exposure of the ionomer/PTFE mixture on the surface owing to the interactions between the two components, as evidenced by the agglomeration observed in the SEM images.

3.2. Effect of PTFE content on H_2 crossover

The measured H_2 volume fraction (Φ_{H2}) decreased as the current density increased at 80 °C and atmospheric pressure (Fig. 3(a)) because of the increase in O_2 evolution (N_{evo,O_2}), according to Eq. (1). Thus, even at low current densities, the anode had a high H_2 content. Conversely, at current densities above 4 A cm^{-2}, Φ_{H2} started to increase again because the supersaturation concentration of dissolved H_2 $\left(C_{H_2}^{super}\right)$ in the ionomer of the cathode CL increased, leading to the permeation of H_2 from

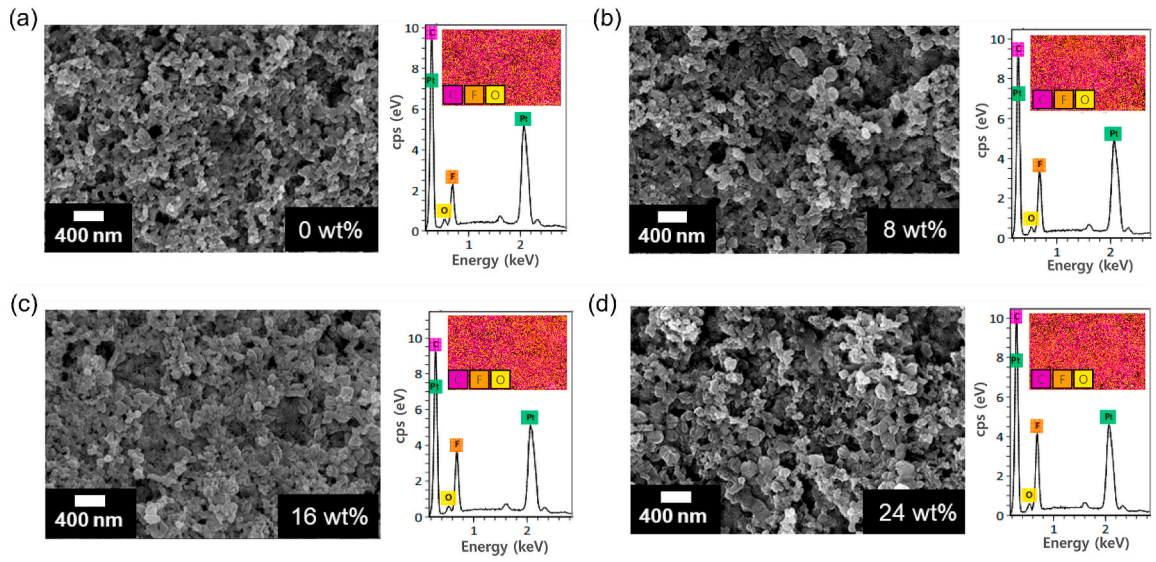

Fig. 2. SEM images and EDS spectra (inset: elemental maps) of cathode catalyst layers with (a) 0, (b) 8, (c) 16, and (d) 24 wt% PTFE.

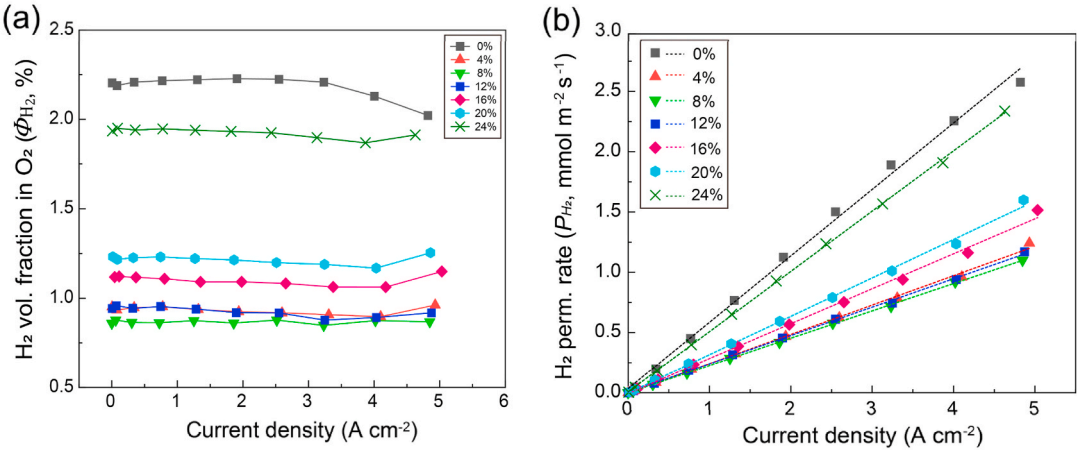

Fig. 3. (a) H_2 volume fraction in O_2 (Φ_{H2}) and (b) H_2 permeation rate (P_{H2}) as functions of the current density at different PTFE contents. The dotted lines represent the P_{H2} derived from the experimental data using Eqs. (4) and (5).

the cathode to the anode. For a straightforward comparison, Fig. S3 presents Φ_{H2} as a function of the voltage. Notably, at 1.5 V, Φ_{H2} decreased from 2.21 % at 0 wt% PTFE to 0.88 % at 8 wt% PTFE. Hence, PEMWEs should be operated at an optimized current density to balance efficiency and safety. Subsequently, the H_2 permeation rate (P_{H2}) was calculated from Φ_{H2} using Eq. (3) (Fig. 3(b)). P_{H2} increased with increasing current density, which aligns with the trend observed in other studies [5,30]. However, the slopes differ, possibly because of differences in the membrane materials and CL structure. The trend in P_{H2} was observed at all PTFE contents, with the lowest P_{H2} observed at 8 wt% PTFE. This low P_{H2} is attributed to the incorporation of PTFE into the cathode CL, which promotes phase-separated ionomer formation and reduces $C_{H_2}^{super}$. Additionally, all MEAs had similar y-intercepts, as expected, because they all used an NR212 membrane and were tested under identical conditions.

The dotted lines in Fig. 3(b) correspond to P_{H2} derived from the experimental data using Eqs. (4) and (5). Fick's first law was applied to estimate P_{H2}, disregarding the lower H_2 concentration at the anode owing to its minimal impact. $C_{H_2}^{super}$ was determined from the cathodic mass balance as outlined in Eq. (4). The sole fitting parameter, the cathodic mass transfer coefficient k_L, is individually determined for each specific cathode CL configuration within the mass balance of cathode (Balance equation in Supplementary data). The P_{H2} data fitted using k_L agreed quite well with the experimental values (Fig. 3(b) and Table 1). k_L varied from 5.4 to 13.7 mm s^{-1} at 0 and 8 wt% PTFE, and the corresponding slopes varied from 0.55 to 0.24 mmol A m^{-2} s^{-1} cm^{-2}, respectively. k_L increased with the addition of PTFE up to 8 wt% (13.7 mm s^{-1}) and then decreased as the PTFE content increased to 24 wt% (5.8 mm s^{-1}). This indicates a reduction in mass transfer resistance with up to 8 wt% PTFE, likely due to alterations in the structure of the catalyst layers. The mass transfer resistance in the cathode CL is affected by the reduction in the pore space and increase in the tortuosity of the pore volume, which obstructs the movement of gas through the pores. Additionally, the ionomer thickness has a significant impact on the mass transport resistance; in a thicker ionomer film, the dissolved H_2 from the catalyst aggregates must traverse longer distances to reach the pore space. To understand the influence of pore structure, the specific pore volume and porosity were determined via mercury intrusion porosimetry (Fig. 4 and Fig. S4). The specific pore volume marginally decreased from 0.77 mL g^{-1} at 0 wt% PTFE to 0.76 mL g^{-1} at 24 wt% PTFE. The porosity followed a similar pattern, decreasing from 53.0 % at 0 wt% PTFE to 51.0 % at 24 wt% PTFE. The total gas transport resistance is typically described as the sum of resistances in the gas diffusion layer (molecular dynamic diffusion), the catalyst layer (Knudsen diffusion),

Table 1
Electrochemical data for membrane electrode assemblies with different PTFE contents.[a]

Ionomer type	PTFE content (%)	Slope of P_{H2} data fitting (mmol m^{-2} s^{-1})/(A cm^{-2})	k_L (mm s^{-1})	Voltage at 5 A cm^{-2} (V)	$C_{H_2}^{super}$ at 3 A cm^{-2} (mol m^{-3})	R_{ohm} (mΩ cm^2)	R_{mt} (mΩ cm^2)	R_{CL} (mΩ cm^2)
D521	0	0.55	5.4	1.86	28.8	53.3	49.1	3.96
	4	0.24	13.1	1.85	12.2	50.2	36.3	–
	8	0.24	13.7	1.84	11.7	49.1	35.8	3.47
	12	0.24	13.2	1.85	12.1	50.6	36.9	–
	16	0.29	11.0	1.84	14.4	49.5	35.4	–
	20	0.32	10.0	1.86	15.8	50.8	35.1	–
	24	0.50	5.8	1.87	26.9	54.0	47.9	7.20

[a] P_{H2}: H_2 permeation rate; k_{mt}: mass transfer coefficient; $C_{H_2}^{super}$: supersaturation concentration of dissolved H_2; R_{ohm}: ohmic resistance; R_{mt}: mass transport resistance; R_{CL}: proton conduction resistance.

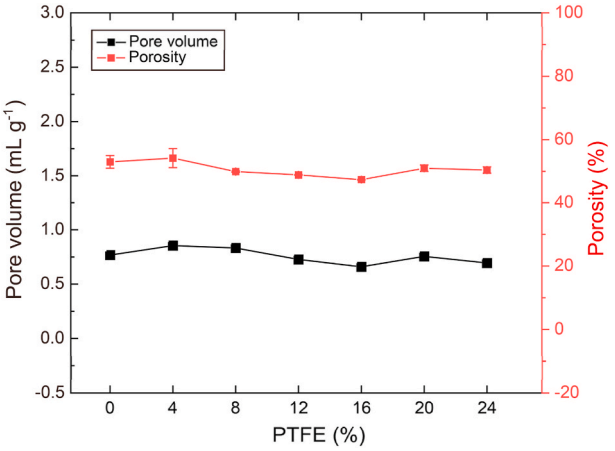

Fig. 4. Pore volumes and porosities of cathode catalyst layers with different PTFE contents.

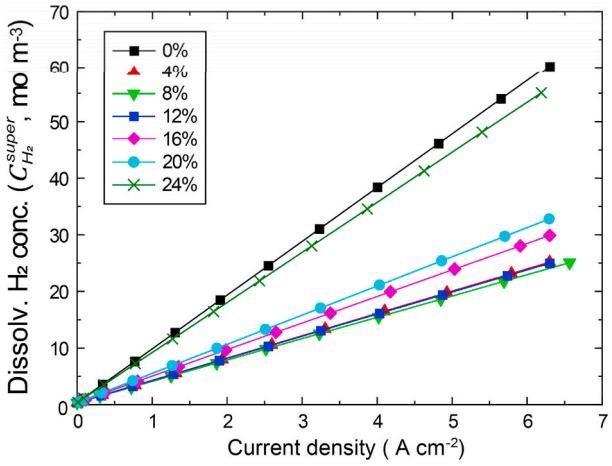

Fig. 5. Concentration of dissolved H_2 ($C_{H_2}^{super}$) as a function of the current density at different PTFE contents.

and the ionomer film. In this study, the transport resistance in the gas diffusion layer does not account for differences in total gas transport resistance because the same gas diffusion layer was used for all MEAs. Within the pore ranges below 0.1 μm in the catalyst layer (CL), gas transport resistance is dominated by Knudsen diffusion. Therefore, the almost similar pore size distribution below 0.1 μm shown in Fig. S4 primarily affects Knudsen diffusion in the cathode CL. Moreover, since the overall pore volume remains similar, the pore distribution in the cathode CL does not impact the total gas transport resistance and H_2 crossover. These findings suggest that the specific pore volume, pore size distribution, porosity of the cathode CL do not significantly influence P_{H2}. Hence, P_{H2} is predominantly determined by the condition of the ionomer in the cathode CL, and the mass transfer resistance of dissolved H_2 toward the ionomer in the cathode CL can be minimized by incorporating PTFE. To further confirm the effect of ionomer on the P_{H2}, we measured the water contact angle of the cathode CL with varying amounts of PTFE as presented in Fig. S5. The results indicate that the 0 % PTFE cathode CL had the highest contact angle at 123.8°, whereas the contact angle decreased to 116.7° in the 8 % PTFE cathode CL, but increased again with the addition of more PTFE. This suggests that the morphology of the ionomer on the surface of cathode CL has a larger hydrophilic area.

P_{H2} is significantly influenced by $C_{H_2}^{super}$ according to Eq. (5). Fig. 5 shows that at high current densities, $C_{H_2}^{super}$ was considerably higher than the saturation concentration of H_2 ($C_{H2}^{sat} = 0.36$ mol m^{-3} at 1 bar_{abs} and 80 °C). This suggests that the H_2 produced during the operation of PEMWEs accumulated in the ionomer of the cathode CL, thus increasing the mass transfer resistance. At all current densities, $C_{H_2}^{super}$ decreased with increasing PTFE content, with the lowest value at 8 wt% PTFE. Specifically, at 3 A cm^{-2}, the $C_{H_2}^{super}$ at 8 wt% PTFE (11.7 mol m^{-3}) is approximately 2.5 times lower than that at 0 wt% PTFE (28.8 mol m^{-3}), despite both MEAs being under supersaturated conditions relative to C_{H2}^{sat}. This disparity increased with increasing current density, leading to an increase in the supersaturated H_2 in the ionomer of the cathode CL. This, in turn, resulted in enhanced H_2 crossover to the anode CL and consequently increased the H_2 concentration in O_2. The incorporation of PTFE influenced phase separation and the morphological properties of the blended ionomer, thereby enhancing H_2 transport through the ionomer and preventing the cathode CL from reaching the H_2 saturation level [31,32].

3.3. Effect of PTFE content on cell performance

The effect of the PTFE content on cell performance was evaluated by measuring the polarization curves. The polarization curves showed that below 3 A cm^{-2}, the cell performance remained nearly the same with increasing PTFE content (Fig. 6(a)), whereas at 5 A cm^{-2}, the voltages of all MEAs, except the MEA with 24 wt% PTFE, were equal to or marginally lower than 1.86 V (Table 1). The minor voltage increase at 24 wt% PTFE was attributed to the PTFE acting as a barrier to mass transport within the cathode CL.

To quantitatively analyze the effect of kinetic behaviors on the power performance, we assessed the iR adjusted cell voltages. This adjustment was made by offsetting the raw voltage measurements with the values of R_{ohm}, obtained through impedance measurements at 1 kHz, effectively removing ohmic polarization from consideration. The operational activation overpotential (η_{act}) of the cell was calculated using the Tafel

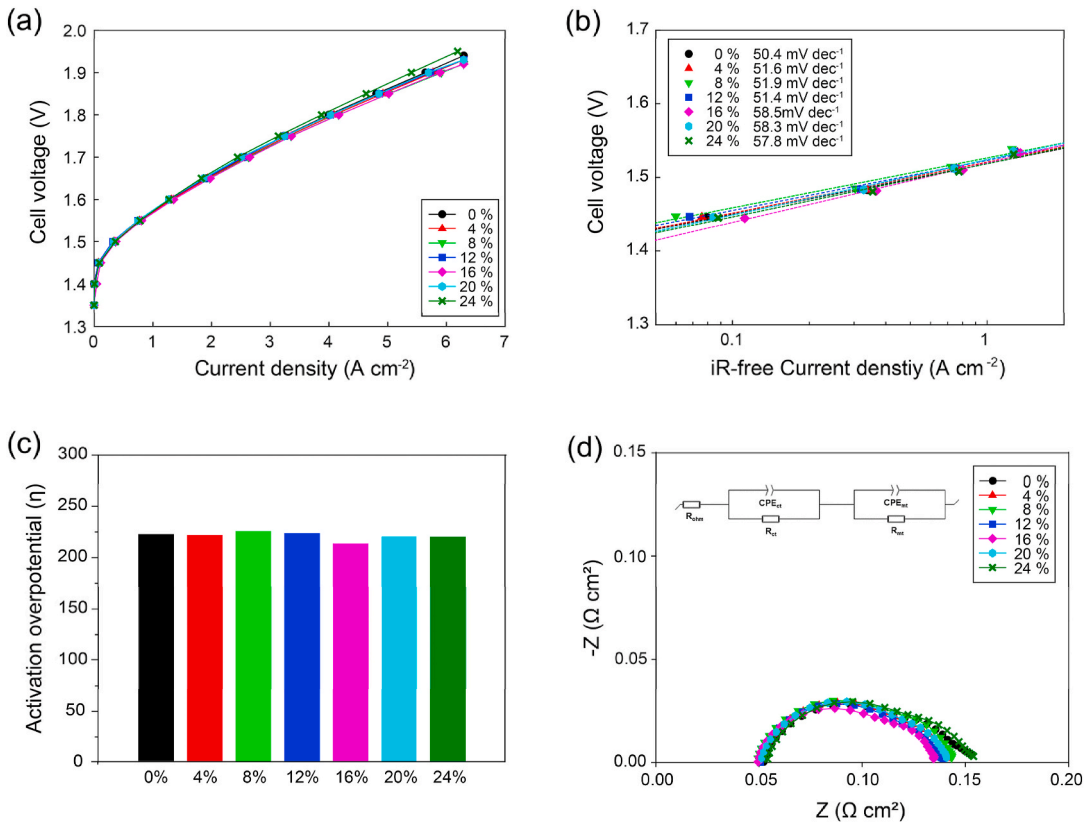

Fig. 6. (a) Polarization curves and (b) Tafel plots with increasing PTFE content in the cathode catalyst layer. (c) Activation overpotential at 0.1 A cm^{-2} and (d) Nyquist plots of membrane-electrode assemblies (MEAs) with different PTFE contents.

equation from the iR-corrected polarization curve shown in Fig. 6(b). This calculation is formulated as $\eta_{act} = a + b \cdot \log(j)$, with b representing the Tafel slope, which is commonly evaluated within a current density range of 0.01–0.1 A cm^{-2}. This range is chosen because, within it, the impacts of both mass transport overpotential and ohmic overpotential can be neglected. According to Fig. 6(b), the Tafel slopes for MEAs with varying levels of PTFE content range from 50.4 mV dec^{-1} (0 wt% PTFE) to 51.4 mV dec^{-1} (12 wt% PTFE), showing only a 2 % difference. This suggests that introducing PTFE to the CCL has minimal effect on the cathodic kinetics of PEMWE up to 12 wt% PTFE, however, when the PTFE content exceeds 12 wt%, the Tafel slope marginally increases at 24 wt% PTFE, reaching 57.8 mV dec^{-1}. This suggests that when the PTFE content exceeds 12 wt%, a thicker PTFE layer may form, which could hinder proton and oxygen transport near the catalyst. Furthermore, as depicted in Fig. 6(c), the activation overpotential at a current density of 0.1 A cm^{-2} across different PTFE-MEAs is comparable, with the maximum variance being less than 10 mV. This indicates that the noticeable differences in performance across these MEAs are not attributable to variations in activation overpotential.

The influence of PTFE on cell performance was further validated via EIS. In Nyquist plots, the intercept on the real axis at high frequency represents the ohmic resistance (R_{ohm}), whereas the intercept of the second semicircle at low frequency is related to the mass transport resistance (R_{mt}). All MEAs had nearly identical R_{ohm}, although the MEAs with 0 and 24 wt% PTFE had higher R_{mt} than the other MEAs (Fig. 6(d) and Table 1). This result indicates that the addition of PTFE does not affect proton conduction within the MEA but enhances mass transport at excess amounts. This was consistent with the polarization data showing a minor decline in cell performance at 24 wt% PTFE. To further explore the effect of PTFE on the proton conduction resistance in the cathode CL (R_{CL}), standalone cathode CLs with 0, 8, and 24 wt% PTFE were prepared and analyzed via EIS in a H_2/N_2 gas mixture. R_{CL} is typically calculated as three times the length between the high-frequency intercept and intercept of the asymptotic line extending from the slightly inclined low-frequency line on the real axis (Fig. S6) [33]. The R_{CL} was 3.96 mΩ cm^2 without PTFE, decreased to 3.47 mΩ cm^2 with 8 wt% PTFE, and slightly increased to 7.20 mΩ cm^2 with 24 wt% PTFE. The reduction in R_{CL} upon the addition of 8 wt% PTFE is attributed to phase separation in the proton-conducting channels, which facilitates smoother proton movement. Nevertheless, these variations in R_{CL} affect the overall performance minimally owing to their significantly lower magnitude compared to R_{ohm}.

3.4. *Effect of ionomer IEC on H_2 crossover*

Cathode CLs were prepared using different ionomer types to analyze the effect of the IEC on the H_2 crossover behavior of PEMWEs. The morphologies of the cathode CLs with D521, D520, 3M800, and 3M725 ionomers were examined via SEM and EDS (Fig. S7). The surface SEM images reveal agglomerates composed of ionomer and catalyst particles, with sizes ranging from several tens to hundreds of nanometers, similar to those observed in the cathode CLs with different PTFE contents. Additionally, the elemental mapping images and EDS spectra showed that the cathode CLs contained C, O, and F. All samples had nearly the same peak intensities because they contained the same amount of perfluorinated sulfonic acid ionomer.

Fig. 7(a) shows Φ_{H2} at various current densities. To facilitate comparison, the variation in Φ_{H2} with respect to the voltage is shown in Fig. S8. Remarkably, Φ_{H2} decreased from 2.21 % in D521-MEA to 1.27 % in D520-MEA at 1.5 V. This slight decrease in Φ_{H2} is attributed to the increase in $N_{evo,}O_2$ with increasing current density. At 80 mA cm^{-2}, the Φ_{H2} values of D521-MEA, D520-MEA, 3M800-MEA, and 3M725-MEA were 2.19 %, 1.27 %, 1.36 %, and 1.38 %, respectively. Except for D521-MEA, the MEAs had Φ_{H2} values below the LEL (4 mol% H_2 in O_2),

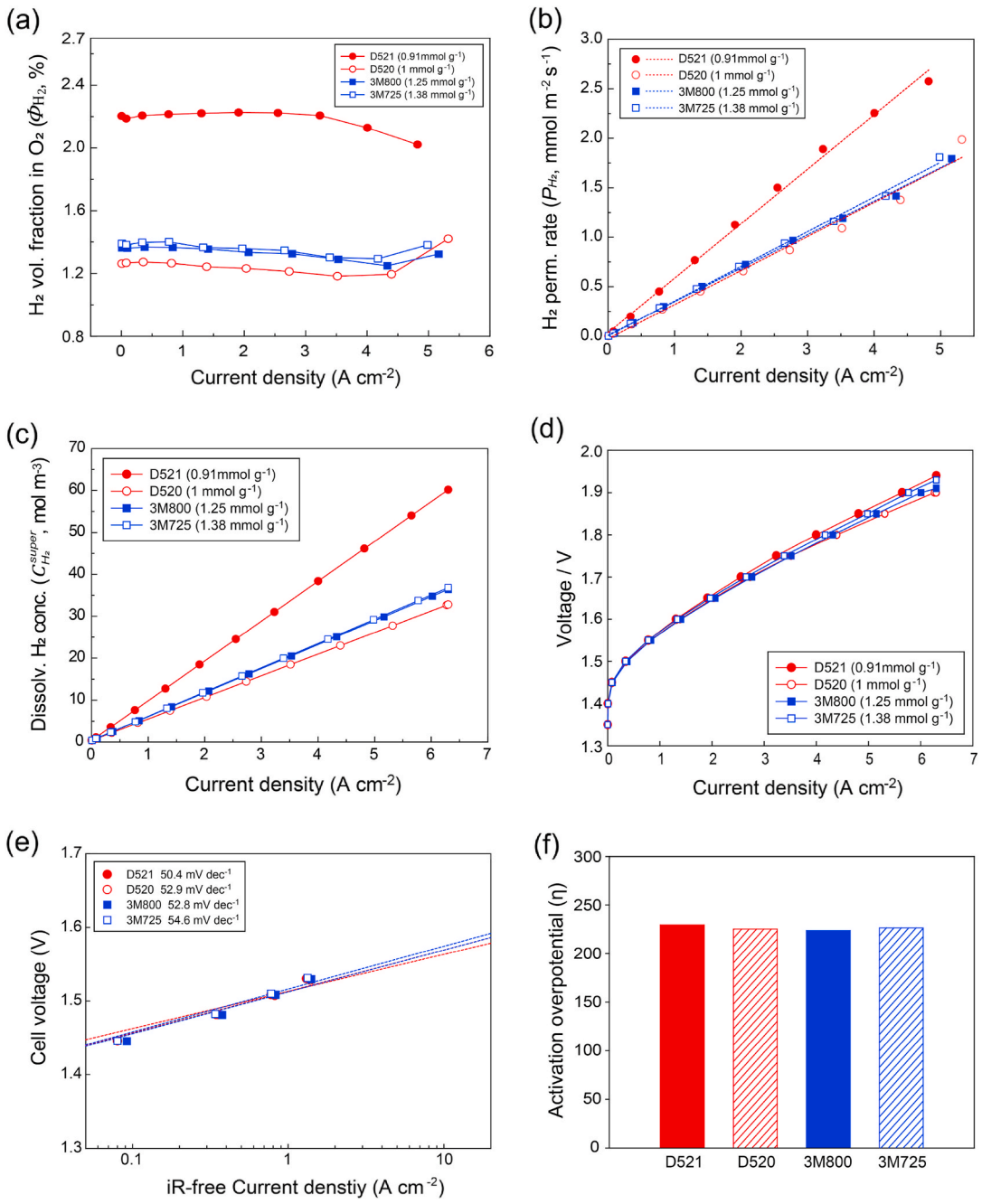

Fig. 7. (a) H_2 volume fraction in O_2 (Φ_{H2}), (b) H_2 permeation rate (P_{H2}), and (c) concentration of dissolved H_2 ($C_{H_2}^{super}$) as functions of the current density for different ionomer types. (d) Polarization curves, Tafel plots, and activation overpotential at 0.1 A cm^{-2} of membrane-electrode assemblies with different ionomer types. The ion exchange capacities of the ionomers are also shown in the figures.

suggesting that the use of a higher-IEC ionomer in the cathode CL of PEMWEs enables safe operation under ambient pressure. Additionally, the trend in P_{H2} with respect to Φ_{H2} was calculated (Eq. (5)) and is presented in Fig. 7(b). The permeabilities of the MEAs were also measured to evaluate the impact of the pore structure on P_{H2} (Fig. S9). The four MEAs displayed only minor differences in permeability, with a maximum difference of 10 % between D521 (133.0 barrer) and 3M725 (145.3 barrer). This indicates that P_{H2} is only marginally affected by changes in the cathode CL pore structure. The gas transport resistance across the CL is typically described as a combination of molecular diffusion, Knudsen diffusion within the CL pores, and transport across the ionomer [34–37]. A minor variation in permeability with respect to the ionomer type was observed, suggesting that the effects of molecular and Knudsen diffusion on the mass transport resistance were minimal. To confirm this explanation, the pore size distribution was measured by mercury intrusion porosimetry. Fig. S10 shows the pore size distribution of the cathode CL based on the type of ionomer, within the range of pore diameters from 0.01 μm to 1 μm. In the diameter range of 0.01 μm–0.1 μm, the gas diffusion resistance is predominantly influenced by Knudsen diffusion. Furthermore, in this range, although the pore volume varies with diameter, the integrated values are similar. This supports the findings in Fig. S9, where the permeability values are similar depending on the type of the ionomer. Therefore, the notable differences in both Φ_{H2} and P_{H2} are primarily attributed to variations in transport across the ionomers. To support these experimental results, we measured the water contact angle and presented in Fig. S11. The water contact angle data

shows that D521, with the lowest IEC, had the highest contact angle at 114.7°. In contrast, D520, 3M800, and 3M725, all with an IEC of 1 or higher, showed contact angles with 123.8°, 115.2°, and 116.4°, respectively. This suggests that the surface morphology of the cathode CL has changed, forming wider hydrophilic channels near an IEC of 1.

Fig. 7(b) shows that P_{H2} increased with increasing current density for all ionomer types, with D520-MEA, 3M800-MEA, and 3M725-MEA having similar lower slopes than D521-MEA. This suggests that D521-MEA exhibited significant H_2 permeation from the cathode to the anode because it had the lowest IEC among the tested ionomers. Because H_2 primarily permeates hydrophilic channels, the low IEC of D521 led to increased supersaturation of dissolved H_2 in the ionomer, facilitating H_2 crossover to the anode and increasing the Φ_{H2} on the anode side [7,10]. To support these findings, the $C_{H_2}^{super}$ in the cathode CL was calculated (Fig. 7(c) and Table 2). For all ionomers, $C_{H_2}^{super}$ was significantly above C_{H2}^{sat} and increased with the current density. This indicates that H_2 produced during electrolysis accumulated within the ionomer, thereby increasing H_2 crossover to the anode. Specifically, at 3 A cm^{-2}, the $C_{H_2}^{super}$ in D521-MEA (28.8 mol m^{-3}) was 1.8 times higher than that in D520-MEA (15.8 mol m^{-3}), despite both values being higher than C_{H2}^{sat}. This result suggests that H_2 permeation through the ionomer is influenced by the morphology of the hydrophilic channels. Increasing the IEC alters the hydrophilic channel structure, thereby affecting the transport of H_2 through the ionomer in the cathode CL.

3.5. Effect of ionomer IEC on cell performance

Fig. 7(d) presents the polarization curves of the MEAs with different types of ionomers. Below 3 A cm^{-2}, the MEAs had similar cell performances, whereas at 5 A cm^{-2}, they showed slight voltage differences. These voltage differences at a higher current density may be attributed to the different IECs of the ionomers, which affect mass transport within the cathode CL by altering $C_{H_2}^{super}$. This hypothesis was tested by conducting EIS measurements (Fig. S12(a) and Table 2). At a higher current density (5 A cm^{-2}), the behavior of the cell was predominantly influenced by the combined effects of R_{ohm} and R_{mt}. The R_{ohm} values of D520-MEA, D521-MEA, 3M800-MEA, and 3M725-MEA were 53.3, 51.7, 50.2, and 51.7 mΩ cm^2, respectively (Fig. S12(a)), showing that differences in R_{ohm} do not significantly affect cell performance.

Consequently, the cell performance at the higher current density was primarily determined by R_{mt}. The R_{mt} of D521-MEA (49.1 mΩ cm^2) was higher than those of D520-MEA (25.9 mΩ cm^2), 3M800-MEA (29.9 mΩ cm^2), and 3M725-MEA (27.9 mΩ cm^2), indicating that the differences in cell performance were due to the mass transport characteristics of the cathode CLs. To investigate the effect of the IEC on proton conduction in the cathode CL, R_{CL} was measured (Fig. S12(b) and Table 2). The values varied from 2.64 to 3.96 mΩ cm^2, which were significantly lower than R_{ohm}, suggesting that R_{CL} had a negligible effect on cell performance.

The activation overpotential (η_{act}) for MEAs using D521, D520, 3M800, and 3M725 was determined through the Tafel equation derived from the iR-free polarization curve as illustrated in Fig. 7(e), defined by the equation $\eta_{act} = a + b \cdot \log(j)$. The calculated Tafel slopes for D521, D520, 3M800, and 3M725 MEAs were 50.4 mV dec^{-1}, 56.3 mV dec^{-1}, 56.7 mV dec^{-1}, and 58.2 mV dec^{-1}, respectively. These values align with those reported in literature [38], indicating that the ion exchange capacity (IEC) of ionomers within the CCL exerts minimal influence on the cathodic reaction kinetics of the PEMWE. A contributory factor to the kinetics is the effective agglomeration of the ionomers and the catalyst. This is supported by the SEM images of the CLs (Fig. S7), which show that the agglomerates are evenly formed and dispersed within the CL. Additionally, as shown in Fig. 7(f), the activation overpotentials at a current density of 0.1 A cm^{-2} for various ionomer-MEAs are similar, with the largest difference being under 10 mV. This similarity suggests that the marked disparities in performance among these MEAs are not due to differences in activation.

Table 2
Electrochemical data for membrane electrode assemblies with different ionomer types.[a]

Ionomer type	Slope of P_{H2} data fitting (mmol m^{-2} s^{-1})/(A cm^{-2})	k_L (mm s^{-1})	Voltage at 5 A cm^{-2} (V)	$C_{H_2}^{super}$ at 3 A cm^{-2} (mol m^{-3})	R_{ohm} (mΩ cm^2)	R_{mt} (mΩ cm^2)	R_{CL} (mΩ cm^2)
D521	0.55	5.4	1.86	28.8	53.3	49.1	3.96
D520	0.34	10.0	1.83	15.8	51.7	25.9	2.64
3M800	0.34	9.0	1.84	17.5	50.2	29.9	3.02
3M725	0.35	8.9	1.85	17.7	51.7	27.9	3.68

[a] P_{H2}: H_2 permeation rate; k_L: mass transfer coefficient; $C_{H_2}^{super}$: supersaturation concentration of dissolved H_2; R_{ohm}: ohmic resistance; R_{mt}: mass transport resistance; R_{CL}: proton conduction resistance.

4. Conclusions

In this study, the cathode CL structure was refined via the incorporation of PTFE as an additive to explore its effect on ionomer characteristics and consequently, the permeation of H_2 from the cathode to the anode. The introduction of 8 wt% PTFE resulted in the lowest H_2 fraction in O_2, which remained below the LEL of 4 mol%. This suggests that the supersaturation concentration of dissolved H_2 ($C_{H_2}^{super}$) at the LEL was minimal. This result is attributed to phase separation in the cathode CL, which leads to well-formed proton-conducting channels within the PTFE/Nafion ionomer through which H_2 can be easily transported. Furthermore, the impact of the IEC of the ionomer in the cathode CL on H_2 crossover was assessed. The D520-MEA exhibited the lowest $C_{H_2}^{super}$ in the cathode CL and the lowest H_2 permeation rate (P_{H2}), demonstrating that ionomers with an IEC greater than 1 mmol g^{-1} are necessary for the safe operation of PEMWEs under ambient pressure. Thus, this investigation offers critical insights for optimizing the cathode CL to ensure safe usage of PEMWEs.

CRediT authorship contribution statement

Inku Kang: Writing – original draft, Methodology, Formal analysis, Data curation, Conceptualization. **Won-Jong Choi:** Writing – original draft, Methodology, Formal analysis, Data curation, Conceptualization. **Hwan Yeop Jeong:** Formal analysis, Data curation. **Chang Jin Lee:** Formal analysis, Data curation. **Soonyong So:** Validation, Methodology, Formal analysis, Data curation. **Duk Man Yu:** Validation, Methodology, Formal analysis, Data curation. **Sang Jun Yoon:** Validation, Methodology, Formal analysis, Data curation. **Hongsuk Kang:** Validation, Methodology, Formal analysis, Data curation. **Dong-Won Kim:** Writing – review & editing, Writing – original draft, Validation, Methodology, Data curation, Conceptualization. **Keun-Hwan Oh:** Writing – review & editing, Writing – original draft, Validation, Methodology, Data curation, Conceptualization.

Declaration of competing interest

The authors declare that they have no known competing financial interests or personal relationships that could have appeared to influence the work reported in this paper.

Data availability

Data will be made available on request.

Acknowledgements

This research was funded by the Korea Research Institute of Chemical Technology (KRICT) Core Research Program (KS2422-20), Repubic of Korea and Korea Research Institute of Chemical Technology (KRICT) Young Researcher Program (BSK24-110), Republic of Korea. This research was also supported by the New Renewable Energy Core Technology Development Project (20223030040220) funded by the Ministry of Trade, Industry and Energy (MOTIE, Republic of Korea), Repubic of Korea.

Appendix A. Supplementary data

Supplementary data to this article can be found online at https://doi.org/10.1016/j.jpowsour.2024.234978.

References

[1] R.-T. Liu, Z.-L. Xu, F.-M. Li, F.-Y. Chen, J.-Y. Yu, Y. Yan, Y. Chen, B.Y. Xia, Chem. Soc. Rev. 52 (2023) 5652–5683.
[2] Y. Chen, C. Liu, J. Xu, C. Xia, P. Wang, B.Y. Xia, Y. Yan, X. Wang, Small Struct. 4 (2023) 2200130.
[3] N. Du, C. Roy, R. Peach, M. Turnbull, S. Thiele, C. Bock, Chem. Rev. 122 (2022) 11830–11895.
[4] C. Rakousky, U. Reimer, K. Wippermann, M. Carmo, W. Lueke, D. Stolten, J. Power Sources 326 (2016) 120–128.
[5] U. Babic, M. Suermann, F.N. Büchi, L. Gubler, T.J. Schmidt, J. Electrochem. Soc. 164 (2017) F387.
[6] P. Trinke, G.P. Keeley, M. Carmo, B. Bensmann, R. Hanke-Rauschenbach, J. Electrochem. Soc. 166 (2019) F465.
[7] C.J. Lee, J. Song, K.S. Yoon, Y. Rho, D.M. Yu, K.-H. Oh, J.Y. Lee, T.-H. Kim, Y. T. Hong, H.-J. Kim, S.J. Yoon, S. So, J. Power Sources 518 (2022) 230772.
[8] A. Martin, D. Abbas, P. Trinke, T. Böhm, M. Bierling, B. Bensmann, S. Thiele, R. Hanke-Rauschenbach, J. Electrochem. Soc. 168 (2021) 094509.
[9] S.-Y. Han, D.M. Yu, Y.-H. Mo, S.M. Ahn, J.Y. Lee, T.-H. Kim, S.J. Yoon, S. Hong, Y. T. Hong, S. So, J. Membr. Sci. 634 (2021) 119370.
[10] M. Schalenbach, M.A. Hoeh, J.T. Gostick, W. Lueke, D. Stolten, J. Phys. Chem. C 119 (2015) 25156–25169.
[11] S. Kim, J. Song, B.T. Duy Nguyen, J. Lee, J. Seong, S. Nam, S. So, J.F. Kim, Chem. Eng. J. 471 (2023) 144696.
[12] S. Giancola, M. Zatoń, Á. Reyes-Carmona, M. Dupont, A. Donnadio, S. Cavaliere, J. Rozière, D.J. Jones, J. Membr. Sci. 570–571 (2019) 69–76.
[13] T. Kim, Y. Sihn, I.-H. Yoon, S.J. Yoon, K. Lee, J.H. Yang, S. So, C.W. Park, ACS Appl. Nano Mater. 4 (2021) 9104–9112.
[14] C. Klose, T. Saatkamp, A. Münchinger, L. Bohn, G. Titvinidze, M. Breitwieser, K.-D. Kreuer, S. Vierrath, Adv. Energy Mater. 10 (2020) 1903995.
[15] T. Sakai, H. Takenaka, N. Wakabayashi, Y. Kawami, E. Torikai, J. Electrochem. Soc. 132 (1985) 1328.
[16] G. Papakonstantinou, K. Sundmacher, Electrochem. Commun. 108 (2019) 106578.
[17] N. Briguglio, S. Siracusano, G. Bonura, D. Sebastián, A.S. Aricò, Appl. Catal. B Environ. 246 (2019) 254–265.
[18] S. Garbe, J. Futter, T.J. Schmidt, L. Gubler, Electrochim. Acta 377 (2021) 138046.
[19] S. Choi, S.-H. Shin, D.-H. Lee, G. Doo, D.W. Lee, J. Hyun, S.H. Yang, D.M. Yu, J. Y. Lee, H.-T. Kim, J. Power Sources 526 (2022) 231146.
[20] A. Albert, A.O. Barnett, M.S. Thomassen, T.J. Schmidt, L. Gubler, ACS Appl. Mater. Interfaces 7 (2015) 22203–22212.
[21] R. Qelibari, E.C. Ortiz, N. van Treel, F. Lombeck, C. Schare, A. Münchinger, N. Dumbadze, G. Titvinidze, C. Klose, S. Vierrath, Adv. Energy Mater. 14 (2024) 2303271.
[22] D. Abbas, A. Martin, P. Trinke, M. Bierling, B. Bensmann, S. Thiele, R. Hanke-Rauschenbach, T. Böhm, J. Electrochem. Soc. 169 (2022) 124514.
[23] H. Ito, N. Miyazaki, M. Ishida, A. Nakano, Int. J. Hydrogen Energy 41 (2016) 20439–20446.
[24] P. Trinke, B. Bensmann, R. Hanke-Rauschenbach, Int. J. Hydrogen Energy 42 (2017) 14355–14366.
[25] M. Schalenbach, Int. J. Hydrogen Energy 41 (2016) 729–732.
[26] D. Bessarabov, P. Millet, in: D. Bessarabov, P. Millet (Eds.), Chapter 5 - Gas Permeation in PEM Water Electrolyzers, PEM Water Electrolysis, Academic Press, 2018, pp. 117–158.
[27] Q. Song, S.K. Nataraj, M.V. Roussenova, J.C. Tan, D.J. Hughes, W. Li, P. Bourgoin, M.A. Alam, A.K. Cheetham, S.A. Al-Muhtaseb, E. Sivaniah, Energy Environ. Sci. 5 (2012) 8359–8369.
[28] S. Ott, A. Orfanidi, H. Schmies, B. Anke, H.N. Nong, J. Hübner, U. Gernert, M. Gliech, M. Lerch, P. Strasser, Nat. Mater. 19 (2020) 77–85.
[29] Q. Zhang, C. Wang, L. Yu, J. You, G. Wei, J. Zhang, Polymers 16 (2024) 668.
[30] E. Kuhnert, M. Heidinger, D. Sandu, V. Hacker, M. Bodner, Membranes 13 (2023) 348.
[31] H. Lin, T.L. Yu, K.-S. Shen, L.-N. Huang, J. Membr. Sci. 237 (2004) 1–7.
[32] M.S. Mu'min, M. Komma, D. Abbas, M. Wagner, A. Krieger, S. Thiele, T. Böhm, J. Kerres, J. Membr. Sci. 685 (2023) 121915.
[33] S. So, K.-H. Oh, J. Power Sources 561 (2023) 232664.
[34] K.-H. Oh, W.-K. Kim, M.-J. Choo, J.-S. Lee, J.-K. Park, H.-T. Kim, Electrochim. Acta 125 (2014) 314–319.
[35] N. Nonoyama, S. Okazaki, A.Z. Weber, Y. Ikogi, T. Yoshida, J. Electrochem. Soc. 158 (2011) B416.
[36] H.S. Kang, K.-W. Nam, S. So, K.-H. Oh, J. Ind. Eng. Chem. 78 (2019) 455–460.
[37] I. Bae, B. Kim, D.-Y. Kim, H. Kim, K.-H. Oh, Renew. Energy 146 (2020) 960–967.
[38] C. Zhao, S. Yuan, X. Cheng, L. An, J. Li, S. Shen, J. Yin, X. Yan, J. Zhang, J. Power Sources 580 (2023) 233413.